

The diurnal variability of atmospheric nitrogen oxides (NO & NO₂) above the Antarctic Plateau driven by atmospheric stability and snow emissions

M. M. Frey¹, N. Brough¹, J. L. France², O. Traulle³, P. S. Anderson¹, M. D. King³, A. E. Jones¹, E. W. Wolff¹, and J. Savarino⁴

¹British Antarctic Survey, Natural Environment Research Council, Cambridge, UK

²Department of Earth Sciences, Royal Holloway, University of London, Egham, UK

³CNRM-GAME, URA 1357, Météo France CNRS, Toulouse, France

⁴Université Joseph Fourier - Grenoble 1 / CNRS-INSU, Laboratoire de Glaciologie et Géophysique de l'Environnement, St. Martin d'Hères, France

Correspondence to: M. M. Frey
(maey@bas.ac.uk)

Abstract

Atmospheric nitrogen oxides (NO and NO₂) were observed at Dome C, East Antarctica (75.1° S, 123.3° E, 3233 m) during austral summer 2009-10. Average ($\pm 1\sigma$) mixing ratios at 1.0m of NO and NO₂, the latter measured for the first time on the East Antarctic Plateau, were 111(± 89) and 102(± 88) pptv, respectively. Mean values are comparable to those at South Pole (Eisele et al., 2008), but in contrast show strong diurnal variability, with a minimum around local noon and a maximum in the early evening. The asymmetry in the diel cycle of NO_x concentrations and likely any other chemical tracer with a photolytic surface source is driven by the diffusivity and height of the atmospheric boundary layer, with the former controlling the magnitude of the vertical flux and the latter the size of the volume snow emissions are diffusing into. In particular, the NO_x emission flux estimated from concentration gradients was on average ($\pm 1\sigma$) of $6.9(\pm 7.2) \times 10^{12}$ molecule m⁻²s⁻¹ and is consistent with the 3-fold increase in mixing ratios in the early evening when the atmospheric boundary layer becomes very shallow. Dome C is likely not representative for the entire East Antarctic Plateau but illustrates the need of accurate descriptions for atmospheric boundary layer physics in atmospheric chemistry models. Calculated mean potential NO₂ production rates from nitrate (NO₃⁻) photolysis are only about 62% of the observed NO_x flux and highlight uncertainties in the parameterization of the photolytic NO_x snow source above Antarctica. A steady-state analysis of the NO₂:NO ratios indicates high concentrations of peroxy radicals (HO₂ + RO₂) in the air above the snow and confirms the existence of a strongly oxidising canopy enveloping the East Antarctic Plateau in summer.

1 Introduction

The nitrogen oxides NO and NO₂ (NO_x) play a key role in determining the oxidizing capacity of the atmospheric boundary layer in the high latitudes. This influence is achieved via photolysis of NO₂, the only source for in situ production of tropospheric

ozone (O_3), through shifting HO_x radical partitioning towards the hydroxyl radical (OH) via the reaction $HO_2 + NO$, and finally through **the latter** also controlling formation rates of peroxides (H_2O_2 & $ROOH$). Atmospheric NO_x concentrations in coastal Antarctica are small, with build up prevented by halogen chemistry (Grannas et al., 2007; Bauguitte et al., 2012), whereas mixing ratios reported from South Pole are unusually high equaling those from the mid-latitudes (Davis et al., 2008). Large mixing ratios of NO_x are, in part, due to significant emissions from surface snow observed at various polar sites. The emissions equal or exceed in magnitude the gas phase source of NO_x (Grannas et al., 2007; Jones et al., 2011, and refs. therein), and are attributed to UV-photolysis of nitrate in snow (Grannas et al., 2007; Frey et al., 2009b). Emissions of NO_x are responsible for significant changes of atmospheric oxidising capacity above snow covered areas: net ozone production was observed in the interior of Antarctica (Crawford et al., 2001; Legrand et al., 2009; Slusher et al., 2010) and unusually high levels of hydroxyl radical levels were detected at South Pole (Davis et al., 2008, and refs. therein). Furthermore, release of NO from snow is associated with the inter-seasonal variability of peroxides above polar snow, since the reaction $HO_2 + NO$ competes with the recombination reaction $HO_2 + HO_2 \rightarrow H_2O_2$ (e.g. Frey et al., 2005, 2009a).

Here we recall the basic gas phase chemistry of NO_x as described by the Leighton mechanism (Leighton, 1961):

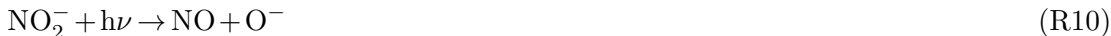


The conversion of NO back to NO_2 via reaction R3 proceeds through additional channels when other oxidants are present, such as hydroxyl (OH), peroxy (RO_2) or halogen (XO, with X = Cl, Br, I) radicals:





NO₂ reacts further to eventually form HNO₃ which is then deposited to the snow surface. The following simplified reaction scheme summarizes currently known NO₃⁻ photochemistry in snow (Grannas et al., 2007):



Major atmospheric chemistry campaigns such as ISCAT and ANTCI at South Pole and CHABLIS at Halley provided the first extensive observations of composition and oxidising capacity of the lower troposphere above Antarctica, including observations of NO_x (Davis et al., 2004b; Eisele et al., 2008; Jones et al., 2008). There is now consensus that NO_x emissions are an essential component of air-snow cycling of oxidised nitrogen species above the polar ice sheets and snow-covered surfaces in the mid-latitudes (Honrath et al., 2000; Grannas et al., 2007; Davis et al., 2008; Frey et al., 2009b). However, the quantitative understanding of NO_x emissions from snow is still incomplete and parameterizations for use in global chemistry-climate models are either non-existent or not reflecting recent progress from lab and field studies.

The study presented here is motivated by the sparse data base of NO₂ observations above snow and a general lack of comparable measurements of NO_x emissions from

surface snow across a wide range of environmental conditions. Reported for the first time are observations of both nitrogen oxides in air above the plateau region of the East Antarctic Ice Sheet (EAIS) and their flux estimated from measurements of concentration gradients. The observed diurnal variabilities of NO_x concentrations are discussed with respect to mixing properties of the atmospheric boundary layer and strength of the snow pack source. Measured NO_x flux is compared to model predictions to diagnose uncertainties in the parameterization of the NO_x source in surface snow. And finally, ratios of atmospheric concentrations of NO_2 and NO are used to infer potential radical concentrations.

2 Methods

Measurements of atmospheric NO_x took place at Dome C, where the year-round operated French-Italian Concordia Station is located (75.1°S , 123.3°E , 3233 m). The local climate is dominated by temperature inversion or katabatic winds that coincide with cold, clear and calm conditions. However, wind speeds are low in comparison to near-coastal areas due to the location on top of a Dome, where surface slopes do not exceed 1%. Occasional synoptic coastal influence coincides with higher wind speeds and brings relatively warmer and cloudier air to the site (e.g. Genthon et al., 2010).

Ancillary data collection included standard meteorology from an automatic weather station at 0.5 km distance (air temperature and relative humidity at 1.6 m, wind speed and direction at 3.3 m), and *insitu* measurements of temperature of air at 1 m and the snow surface, broad band UV-A radiation (UVA CUV4 broadband radiometer, Kipp & Zonen), atmospheric turbulence observations from a **sonic anemometer** at 1 km distance and **surface ozone**. All times are given as local time (LT), equivalent to UTC+8 h.

2.1 NO_x detection

For NO_x detection a 2-channel chemiluminescence detector (CLD) was used that was run previously year-round at Halley (75.6° S, 26.6° W, 37 m) in coastal Antarctica (Bauguitte et al., 2012). One channel of the CLD measured atmospheric NO whereas the other determined the sum of NO and NO₂ originating from the quantitative photolytic conversion of NO₂. The signal difference between the two channels was then used to calculate atmospheric NO₂ concentrations. The instrument was operated out of an electrically heated Weatherhaven tent located in the designated clean-air sector 0.7 km upwind (South) of Concordia station. Apart from snow drift due to the tent structure the surrounding snow pack had not been subject to any perturbations such as motorized vehicle or foot traffic for the past 4-5 yr. Three 20 m-long intake lines (Fluoroline 4200 high purity PFA, I.D. 4.0 mm) were mounted on a mast about 15 m upwind outside the snow drift zone to sample air at 0.01, 1.00 and 4.00 m above the natural snow pack. During selected time periods firn air was sampled by inserting one inlet into pre-cored horizontal holes at 5-10 cm snow depth.

The sample intakes were shielded from solar radiation with black heat-shrink tubing and connected inside the Weatherhaven tent to a valve box, which automatically switched the CLD between sampling heights on a 90 s duty cycle. In order to achieve continuous flow and reduce sample residence time in the tubing, ambient air was drawn through each one of the long intake lines at 5.0 STP-Lmin⁻¹ using high-capacity vacuum diaphragm pumps (GAST, Part No. DOA-P725-BN). The CLD inlet drawing sample air from the respective intake line was mass-flow controlled at 1.0 STP-Lmin⁻¹ for each channel. Spike tests using the NO gas standard showed that air sample residence time between the tip of the sample intake and the reaction vessel inside the CLD was 4 s, and therefore < 2 s in the photolytic cell. On three occasions ambient air was sampled for up to 1.5 h through all three inlets mounted at 1.00 m above the snow. Parametric (two-sample t-test) and non-parametric tests (Wilcoxon signed rank test) performed on NO and NO₂ mixing ratios did not show any significant differences

between the inlets at the 95% confidence level.

Transforming CLD count rates into atmospheric mixing ratios required regular measurement of baseline, instrument sensitivity, conversion efficiency (CE) of R1 taking place in the photolytic converter and detector artefacts (Table 1). Baseline count rates were measured for 60s every 13.5 min alternating between all three inlets, i.e. implying a repeat period of 40.5 min for each individual intake line. Instrument sensitivity and CE were determined every 14h based on addition of a 4 ppbv **NO standard to the sampled air flow**. Some of the automated calibrations were compromised by a small leak and the respective CLD sensitivities were then replaced by average values confirmed by pre- and post-season calibrations.

The **detector artefact** was measured every 14h, offset by 7h to the calibration runs. CE was on average 0.30 (range 0.25 - 0.35) (Table 1), thus considerably lower than a CE of 0.5 reported for the same instrument operated at sea level (Bauguitte et al., 2012). We explain this as follows: if one neglects oxidants in ambient air CE depends solely on the photolysis rate j and sample residence time τ in the photolytic cell of the CLD (Ryerson et al., 2000):

$$CE = 1 - e^{-j\tau} \quad (1)$$

The former is a function of the optical geometry of the instrument, which had remained unchanged, whereas the latter decreases with altitude since the photolytic cell was not pressure controlled. Mean ambient pressure (650 mbar) and temperature (269 K) at Dome C result in a volumetric flow rate about 0.72 that at Halley. Inserting into the equation above the respective values for Dome C (DC) and Halley and taking the ratio yields

$$\frac{\tau_{DC}}{\tau_{Halley}} = \frac{\ln(1 - CE_{DC})}{\ln(1 - CE_{Halley})} \quad (2)$$

With CE_H of 0.5 and a ratio of τ_{DC}/τ_{Halley} of 0.72 one obtains a CE_{DC} of 0.4. Contrary to the Halley measurements we used continuously long sample intake lines, which causes

the pressure inside the photolytic cell to drop well below ambient levels. A pressure drop of 250 mbar, which seems reasonable, would then resolve the remaining discrepancy with the observed CE_{DC} .

2.2 NO_x data processing and uncertainty

5 The linearly interpolated signal of all baseline intervals was subtracted from the CLD count rates recorded at 1 Hz. The baseline levels were typically the same in between the three inlets, but showed large and systematic variations when NO_x concentrations between the three inlets were very different, i.e. when either near-surface gradients were pronounced during certain times of the day or when firm air was sampled. During these 10 sampling periods the signals from each inlet were corrected individually by subtracting only the baseline interval corresponding to the specific inlet. The repeat period of baseline measurement for the individual inlet increased therefore to 40.5 minutes. An artefact correction was applied during the 11-Dec-2009 to 3-Jan-2010 period, amounting to 6-8 pptv and 3-4 pptv for NO and NO₂, respectively (Table 1). After 4-Jan-2010 15 artefact levels dropped to about 50% of the above values and were not used.

Shielding an air sample from solar radiation once entering the sample line can potentially alter the ratio of NO₂ and NO as the Leighton photostationary state (R1-R3) shifts to a new equilibrium. Formation of NO₂ from reaction R3 at Dome C during this study was estimated to be 4×10^6 molecule cm⁻³ s⁻¹. With a sample residence time in the inlets of <4 s one obtains median changes in NO and NO₂ of <1.6 % and therefore 20 no correction was applied.

The mean wind direction during the field campaign was from SSW (208°) with an average speed of 2.6 ms⁻¹. During less than 1 % of measurement time the wind came from Concordia station carrying polluted air from the station power generator to the measurement site. To remove pollution spikes a moving 1-min standard deviation filter 25 was applied rejecting data when 1- σ of NO and NO₂ mixing ratios exceeded 24 and 90 pptv, respectively. Comparison to logged contamination events and the above wind rose analysis confirmed the efficiency of the statistical filter in suppressing any pollution

episode either from power generators at Concordia station or occasional vehicle traffic (air planes, snowmobiles).

Filtered data, still including some negative values in the case of NO_2 , were then aggregated to 1 min averages. About 6.3% of all mixing ratios of NO_2 , equivalent to 65 h, were still negative due to uncertainties in baseline and artefact determinations and were discarded. The uncertainty in the 1-minute averages due to random errors was estimated as the standard error (standard deviation of the mean) and amounted to 1 and 11 pptv for NO and NO_2 , respectively (Table 1). The precisions or fractional uncertainties were 2.6 and 43.6 % for NO and NO_2 , respectively (Table 1). The errors in NO_2 are larger than seen previously and are due to the reduced conversion efficiency at Dome C.

Quantification of NO_2 as NO after photolytic conversion can be compromised by the presence of other chemical gas phase species, which produce NO in the photolytic converter, i.e. whose absorption cross sections have significant overlap with that of NO_2 (Fig. 1a,b). Interferents relevant for our system are bromine nitrate (BrONO_2) and nitrous acid (HONO) (Ryerson et al., 2000), of which only the latter is expected to play a role on the EAIS plateau during polar day. We therefore calculated a potential interference as the ratio of the respective photolysis rates, $j_{\text{HONO}}/j_{\text{NO}_2}$, in the photolytic converter (Fig. 1c) and obtained a value of 0.22, somewhat smaller than that of 0.37 estimated for a similar instrument (Ryerson et al., 2000). HONO was previously observed at South Pole in Summer using laser-induced fluorescence and showed median levels of 5.8 pptv (maximum 18.2 pptv) (Liao et al., 2006). If similar levels of HONO are present at Dome C, then the seasonal mean of NO_2 at 1.0 m of 102 pptv (Table 2) would be overestimated by 1.3% (maximum 4.1%). More recent HONO measurements at Dome C report a range of 5-60 pptv, and corrections would be correspondingly larger if interferents in the wet chemical method employed can be ruled out (Kerbrat et al., 2012).

2.3 NO_x flux estimates

We derived NO_x flux based on the integrated flux gradient method (e.g. Lenschow, 1995), as briefly outlined below. Fick's Law describes how concentration gradient $\partial c/\partial z$ and diffusion coefficient K_c of a chemical tracer relate to its diffusive flux F .

$$F = -K_c \frac{\partial c}{\partial z} \quad (3)$$

Within the atmospheric boundary layer, vertical diffusion is dominated by turbulent mixing, rather than molecular diffusion, and K_c can be estimated by a variety of methods from analogous measurements of the turbulent diffusivity for momentum K_m and heat K_h . In this study, we used sonic anemometer measurements of atmospheric turbulence available from a tower at 0.8 km distance, since *in situ* observations were compromised due to instrument malfunctioning. K values are calculated according to the Monin-Obukhov similarity theory (MOST) whose predictions of flux-profile relationships at Halley, an Antarctic coastal site of the same latitude as DC, agree well with observations (Anderson and Neff, 2008, and references therein). For the chemical flux estimate we make the assumption that $K_c \sim K_h$. The NO_x flux F is then given by

$$F = -\frac{\kappa u_* z}{\Phi_h\left(\frac{z}{L}\right)} \frac{\partial c}{\partial z} \quad (4)$$

where κ (set to 0.40) is the von Karman constant, u_* is the friction velocity, z is height, and $\Phi_h\left(\frac{z}{L}\right)$ an empirically determined stability function for heat with L as the Monin-Obukhov length. Assuming constant flux across the layer between the two measurement heights z_1 and z_2 allows to integrate and yields

$$F = -\frac{\int_{c_1}^{c_2} \kappa u_* \partial c}{\int_{z_1}^{z_2} \Phi_h\left(\frac{z}{L}\right) \frac{\partial z}{z}} = -\frac{\kappa u_* [c(z_2) - c(z_1)]}{\int_{z_1}^{z_2} \Phi_h\left(\frac{z}{L}\right) \frac{\partial z}{z}} \quad (5)$$

Stability functions used were $\Phi_h = Pr_t + 4.62z/L$ established previously for stable conditions above snow (King and Anderson, 1994) and $\Phi_h = Pr_t(1 - 11.6z/L)^{-0.5}$ for

unstable conditions (Hoegstroem, 1988), where the Prandtl number Pr_t is set to 0.95. Note that in the neutral boundary layer Φ_h is Pr_t and the denominator in Eq. 5 simplifies to $Pr_t \ln(z_2/z_1)$. Friction velocity u_* and L were computed from high frequency (10 Hz) measurements of the three-dimensional wind components (u , v , w) and temperature by a sonic anemometer (ATEC1-061101) mounted at 7 m above the snow on a tower at 1 km distance. Processing in 10-minute blocks included despiking, temperature cross-wind correction and a double coordinate rotation to force mean w to zero (Kaimal and Finnigan, 1994; Van Dijk et al., 2006). The instrument alternated between 5 minutes of measurements and 12 minutes of heating to prevent frost build up on the sensors. Eq. 5 implies that positive flux points in upward direction, equivalent to snow pack emissions and vice versa, equivalent to deposition.

The application of MOST and the assumption of constant flux both require a chemical lifetime much longer than the mixing time scale of the respective tracer. This does not hold true for NO and NO₂, which are subject to rapid interconversion. However, in the case of NO_x previous estimates of chemical lifetime range between 6.4 h (daily mean) at Halley (Bauguitte et al., 2012) and 8 h (median) at South Pole (Davis et al., 2004a), whereas the mixing time scale, e.g. estimated as the ratio z_2/u_* , was during this study on average only on the order of seconds. We therefore limit ourselves to deriving only NO_x flux.

It should be noted that application of the flux-gradient method is only possible, when concentration gradients $\Delta[\text{NO}_x]$ can be detected. 10-minute averages of $\Delta[\text{NO}_x]$ not significantly different from zero, i.e. smaller than their respective 1- σ standard error were therefore not included in the flux estimates (Fig. 4). The total uncertainty of the 10-minute NO_x flux due to random error in $\Delta[\text{NO}_x]$ (31%), u_* (3% after Bauguitte et al. (2012)) and measurement height (error in $\ln z_2/z_1$ of $\sim 7\%$) amounts to 32%. This reduces to 13% when considering 1-hr flux averages.

3 Results

Mixing ratios of atmospheric NO and NO₂ were measured at up to three levels above the snow surface from 10 December 2009 to 28 January 2010 (Fig. 2,3) and show at 1.0 m for the entire season a median of 84 and 74 pptv, respectively (Table 2). The highest mixing ratios are detected in firn interstitial air and systematically decrease with sampling height above the snow surface. For example, median levels of NO_x were 168, 145 and 135 pptv at 0.01, 1.0 and 4.0 m, respectively, whereas the median of available samples in firn air was 371 pptv (Table 2). Furthermore, examination of the median NO₂:NO ratio reveals also a dependency on height with a decrease from 1.5 in firn air to 0.7 at 1 m above the snow surface (Fig. 2,3, Table 2).

Mixing ratios of NO and NO₂ show strong diurnal variability out of phase with solar radiation, with a daily minimum occurring around local noon and a maximum in the evening/night time hours (Fig. 3,7). Build up and decay of the daily maximum mixing ratios follow on calm days a repeatable pattern, with changes always starting at the lowest intake level followed by those aloft (Fig. 3b,c). On a number of days in December and more frequently in January NO_x mixing ratios decreased and the diurnal cycle was suppressed concurrent with wind speeds above 5 ms⁻¹ (Fig. 2), which however does not alter much the median diurnal cycle at Dome C (Fig. 7). Comparison of the two-week medians of atmospheric NO_x mixing ratios reveal a decreasing seasonal trend. For example, NO_x mixing ratios at 1.0 m are with 388 pptv highest before the summer solstice during 1–15 December and then decrease via 159, 139, to 128 pptv in the second half of January. Comparison of median NO concentrations shows that also at South Pole the highest atmospheric mixing ratios are observed in early summer, i.e. the second half of November (Table 3).

The mean NO_x mixing ratio difference $\Delta[\text{NO}_x]$ between 1 and 0.01 m was -50 pptv with an average standard error of 9 pptv (Fig. 4a). About 14.5% of the available 10-minute $\Delta[\text{NO}_x]$ averages, observed typically around local noon, a time of strong atmospheric mixing, were not significantly different from zero and therefore excluded

from the flux estimate (Fig. 4a). From a total of 1356 10-minute average flux values (~ 10 days), 52% were during stable and the remainder during unstable conditions. Corrections from Φ_h decreased (increased) flux during stable (unstable) conditions by $<10\%$ when compared to the case of a neutral boundary layer. The NO_x fluxes were almost exclusively emissions from the snow surface with an average ($\pm 1\sigma$) of $6.9(\pm 7.2) \times 10^{12}$ molecule $\text{m}^{-2}\text{s}^{-1}$ (Table 2, Fig. 4c).

4 Discussion

This study reports the first time direct observations of NO_2 in the interior of Antarctica and the longest NO_x flux measurements above snow on the continent. A first look at absolute atmospheric concentrations shows that the NO_x mixing ratios observed at Dome C are highly elevated. For example, median NO mixing ratios of 81–123 pptv in December are about an order of magnitude higher than at other polar sites (Halley, Neumayer, Alert, Barrow or Summit, as reviewed in Grannas et al. (2007)), but fall into the range observed on an airborne campaign across EAIS and at South Pole during some summer seasons (Table 3). However, a striking difference to South Pole is the pronounced diel cycle of NO_x out of phase with solar radiation, which will be discussed below in more detail.

4.1 Diurnal variability of NO_x and boundary layer stability

If the photolytic snow source of NO_x was the main driver of atmospheric concentrations one might expect a daily NO_x cycle closely associated with solar irradiance. However, the diurnal NO_x variability on calm days lacks any correlation with UV irradiance (e.g. Fig. 8a) and shows a peculiar asymmetry of the maximum with respect to solar noon (Fig. 3,7). Even though this daily pattern is disrupted at elevated wind speeds, it is preserved in the median diurnal cycle of NO and NO_2 for the entire season (Fig. 7). This indicates that the boundary layer might play an important role in controlling

concentrations of chemical tracers emitted at the surface, as suggested by previous micrometeorological studies at Dome C (Argentini et al., 2005; King et al., 2006).

Firstly, it is important to note that at Dome C air temperature and wind speed exhibit a strong diurnal cycle (Fig. 2a, 3a), as observed by King et al. (2006). The air temperature shows daily maxima in the early afternoon, lagging that of solar radiation by about 2 h, and has an amplitude of ~ 12 K (Fig. 3a). The wind speed peaks around noon, decreases in the early evening, but picks up again during night time, with a rather small daily amplitude of ~ 1.5 ms^{-1} (Fig. 3a). Diurnal variations of both parameters are typical for locations where a convective boundary layer develops as a response to daytime heating (King et al., 2006). Not only wind speed but also wind direction shows a small but significant diurnal cycle. Winds were from 190 - 200° during 1000 - 1400 LT and then shift to $\sim 220^\circ$ during 1800 - 2400 LT. Both, increase in wind speed and change of wind direction later in the evening suggest development of an Ekman spiral consistent with previous findings at Plateau Station on the EAIS (Kuhn et al., 1977).

Secondly, boundary layer parameters that can be derived from direct turbulence measurements include u_* , L and K and contribute to a more complete picture of mixing processes. The friction velocity u_* measures how efficiently a trace gas emitted at the surface is mixed vertically into the atmospheric boundary layer. The median diurnal cycle of u_* peaks around local noon and drops during night time hours (Fig. 5a). The Monin-Obukhov length L is a height proportional to the height above the surface at which buoyancy first dominates wind shear, with negative (positive) L values indicating unstable (stable) conditions. The characteristic diurnal cycle of L during the study period suggests that between 0700 and 1600 LT the boundary layer becomes unstable and convective, whereas during the rest of the day stable stratification prevails (Fig. 5b), consistent with previous micrometeorological measurements (Argentini et al., 2005; King et al., 2006). And finally, knowing u_* and L allows to calculate the turbulent diffusion coefficient for heat K_h at a given height as defined in eq. 4. K_h correlates with horizontal wind speeds and its diurnal cycle looks very similar to that of u_* (Fig. 4b,5c). The above suggests that mixing is strongest around solar noon and has then contributions

from turbulence due to buoyancy (free convection), whereas during night time (1800-0600 LT) the atmosphere is stably stratified and turbulence due to wind shear (forced convection) is the sole driver of mixing.

These observations confirm the daily development of a convective boundary layer at Dome C in summer, which had been found previously based on sodar records (Argentini et al., 2005) and quantification of the surface energy budget, with the average diurnal sensible heat flux being in upward direction (i.e. < 0) during 0600-1700 LT (King et al., 2006). At its origin is the greater partitioning of available energy into the sensible heat flux rather than latent heat because air temperatures and therefore water vapour pressures are low at this location (King et al., 2006). The sensible heat flux is responsible for the large day-night temperature amplitude and drives the development of a convective boundary layer throughout the day, giving thereby rise to efficient vertical mixing (King et al., 2006). Implications for NO_x mixing ratios are illustrated by the inverse relationship with K_h , and therefore u_* : NO_x mixing ratios are small around local noon when efficient convective mixing takes place and increase during the night, when K_h is small (Fig. 6a). A similar non-linear relationship has been observed previously at South Pole between NO and u_* (Neff et al., 2008).

Thirdly, the mixing height H of the boundary layer is another parameter, important for chemical budget calculations, as it determines the available air volume snow emissions can diffuse into and which was observed to show significant diurnal variability at Dome C (King et al., 2006). We estimated H using the parameterizations by Pollard et al. (1973) and Zilitinkevitch et al. (2002) described previously for analysis of boundary layer behaviour at South Pole (Neff et al., 2008). Since diurnal cycles are present at Dome C the use of these simple scaling laws warrants caution as they apply to the stable or weakly unstable boundary layer and assume that an equilibrium boundary layer depth is reached. Nevertheless, the parameterization after Pollard et al. (1973) compared well with observed profiles at Summit/Greenland (Cohen et al., 2007), a site of similar diurnal radiative forcing at the top of the atmosphere and also at South Pole during very stable conditions with $H < 50$ m (Neff et al., 2008). A significant diurnal variability is

found and daily ranges of median H were 5-55 m and 17-165 m, after Pollard et al. (1973) and Zilitinkevitch et al. (2002), respectively (Fig. 5d). No direct observations of H are available to validate the estimates. However, the sodar records from summer 1999 showed that starting from a shallow nocturnal boundary layer of <50 m at 0700 LT a capping inversion reached heights of 200-300 m at 1300-1400 LT in late December to early January and disappeared by 1800 LT leaving behind the nocturnal boundary layer (Argentini et al., 2005; King et al., 2006). Thus, our H predictions are likely biased low during unstable conditions, but suggest during stable conditions the existence of a very shallow nocturnal boundary layer with $H < 20$ m (Fig. 5c). This is consistent with visual observations of a defined layer of haze forming at the ground at Dome C, which indicate that the atmospheric boundary layer does not exceed building height of 20 m during night time. A shallow boundary layer is typically associated with elevated NO_x (Fig. 6b), as seen also at South Pole (Neff et al., 2008). It should be noted that a correlation between estimated H and atmospheric concentration is expected, since the above parameterizations of H depend strongly on friction velocity. This implies that it is the diffusivity of the atmosphere which controls both concentration gradients and the extent of boundary layer height H . The latter is needed in atmospheric chemistry applications to assess the impact of snow emissions on the atmospheric budget and compare to gas phase production rates.

The diel cycles of all parameters based on MOST and related to the diffusivity of the lower atmosphere at Dome C (u_* , L , K_h and H) are asymmetrical around local noon (Fig. 3c,5). They increase gradually in the morning, whereas they decrease more quickly in the early evening, illustrating the development and collapse of the convective boundary layer. The daily variability in mixing properties of the lower atmosphere is clearly reflected in the asymmetry of the diel NO_x cycle, which shows large increases in the evening but lacks a discernible peak in the morning (Fig. 3).

Examination of wind speed and temperature profiles confirms the impact of atmospheric stability on the diurnal variability of NO_x mixing ratios. During the relatively calm period Jan 1-4 near-surface gradients of temperature, i.e. between air tempera-

ture measured at 1 m above the snow and the snow-surface temperature, show a similar asymmetry: as expected, warming and cooling of air always initiate at the surface, but gradients of temperature are consistently larger in the evening than in the morning (Fig. 3). Mixing ratios of NO_x mimic that behaviour, as changes (increase or decrease) always initiate at the surface (Fig. 3b,c). To analyse this further we calculate the bulk Richardson number Ri_b , a parameter used in profile methods and not subject to the assumptions of MOST. Ri_b is the ratio of temperature and wind speed gradients and describes the ratio of turbulence due to buoyancy (free convection) relative to that due to shear (forced convection) (Jacobson, 1999):

$$Ri_b = \frac{g[\theta_v(z_r) - \theta_v(z_0)](z_r - z_0)}{\theta_v(z_0)[u(z_r)^2 + v(z_r)^2]} \quad (6)$$

with gravitational acceleration g , potential virtual temperature θ_v , measurement heights $z_{r,0}$, and horizontal wind speed components u and v . Wind speed measurements at 3.3 m were scaled to 1.0 m assuming a logarithmic wind profile and by definition wind speed at z_0 is zero. Throughout most of the day Ri_b is positive, equivalent to weakly to very stable conditions (Fig. 3b, 7). Small and negative Ri_b values around solar noon indicate that the atmosphere has become unstable with most turbulence from wind shear, but some contributions also from buoyancy (Fig. 7). The Ri_b approach significantly underestimates the daily duration of convective behaviour when compared to the above analysis of L or existing observations Argentini et al. (2005). We attribute this to systematic errors in the calculation of Ri_b due to the uncertainty in the temperature gradients. This is the case during near neutral and unstable conditions when gradients are small compared to the temperature measurement error of $\sim 0.5^\circ\text{C}$. During stable conditions this should be less important. In the early evening Ri_b rises sharply to a maximum around 1830 LT, preceding that of NO_x mixing ratios by about 1 h. The increase illustrates the drop in wind shear concurrent with a strong temperature inversion at the surface. Turbulent flow is very reduced, possibly even to laminar flow. The maximum in Ri_b coincides with a sharp increase in mixing ratios of NO_x (Fig. 3b, 7).

Later on Ri_b decreases again as wind shear grows, leading to upward mixing of NO_x accumulated near the ground. NO mixing ratios decrease at a quicker rate than mixing ratios of NO_2 , also reflecting that photolysis of NO_2 (R1) is reduced at higher solar zenith angles (Fig. 3b, 7).

5 Since the diurnal cycle of sensible heat flux was observed to be fairly symmetrical around noon (see King et al., 2006), the asymmetry in the temperature gradients must be then due to differences in diffusivity of heat K_h between the morning and evening situation. Indeed, small temperature gradients in the morning are consistent with larger K_h values when compared to the same hour of day in the evening and illustrate that
10 convection is a very efficient process for the upward mixing of heat. In the evening the downward heat flux is smaller due to comparatively lower diffusivities. The assumption that heat is more effectively moved in upward direction away from the snow surface than towards it is confirmed by the asymmetry in average snow heat flux which had been found to show a minimum of -30 W m^{-2} at 0800 LT (outgoing flux) compared to
15 a maximum of 20 W m^{-2} at 1800–2300 LT (incoming) (King et al., 2006). By assuming similarity between K_h and K_c the same argument applies ~~than~~ also to NO_x gradients and flux.

Direct and profile methods have uncertainties. For example, the application of MOST is limited during very stable conditions and likely causes an overestimate of K_h and
20 corresponding flux during the early evening hours. Conversely, Ri_b captures well the asymmetry in atmospheric diffusivity which must be present to explain the NO_x cycle, but underestimates strength and duration of convection due to systematic errors. Despite of these shortcomings both direct and profile methods suggest that diurnal changes in atmospheric NO_x mixing ratios are driven by the diel cycle of atmospheric stability.

25 Comparison of diurnal cycles of NO_x mixing ratios with Summit/Greenland and Halley in coastal Antarctica is informative as both sites are located at similar latitudes as Dome C and therefore subject to the same diurnal radiative forcing at the top of the atmosphere. However, at Summit, NO_x mixing ratios are not only lower, but show two daily maxima, one in the morning and one in the evening, about equal in size (Thomas

et al., 2011). Two daily maxima are consistent with a stability analysis based on profile measurements that revealed a symmetric diurnal cycle of Ri_b , e.g. unstable conditions during the day ($Ri_b < 0$) and stable conditions ($Ri_b > 0$) during the night (Helmig et al., 2002). At Halley, the diurnal cycle of NO_x mixing ratios follows with some delay solar irradiance. In contrast to Dome C, no convection occurs and during calm periods the boundary layer height remains almost constant throughout the day (King et al., 2006). Mixing in the boundary layer is exclusively driven by wind shear and depends therefore more on synoptic events (King et al., 2006). The diurnal cycle of NO_x mixing ratios is controlled by the snow source and atmospheric halogen mediated chemistry, i.e. formation and uptake of BrNO_3 and INO_3 , which prevents build up of NO_x (Bauguitte et al., 2012).

4.2 The NO_x snow source

The 10 minute averages of observed NO_x flux show some scatter due to noise present in concentration gradients and K_h values (Fig. 4c, 8c), but exhibit a close relationship with solar irradiance and atmospheric diffusivity (Fig. 8), as also seen in the median diurnal cycle for the entire observational period (Fig. 9b). The observation that mixing ratios of NO_x in firn air correlate with surface UV irradiance, albeit on some days with a time lag of a few hours (Fig. 8a), confirms that the NO_x emission flux originates from a photolytic source in the upper snow pack, i.e. the photolysis of nitrate (NO_3^-) in snow. However, the fate of the emissions is then strongly controlled by atmospheric diffusivity. Noon time NO_x flux is typically three times larger than that during night time (Fig. 9b), a diel pattern that is occasionally disrupted when the diffusivity of the boundary layer increases leading also to larger NO_x flux values (Fig. 8b). The median NO_x reveals also a small secondary flux maximum during night time, which is driven entirely by wind shear (Fig. 9). Generally, maximum NO_x flux coincides with minimum atmospheric mixing ratios, consistent with the notion that as the mixed boundary layer develops emissions diffuse into an increasingly larger volume (Fig. 9).

Assuming that NO_x snow emissions are uniformly mixed throughout the boundary

layer and that the main NO_x loss is $\text{NO}_2 + \text{OH}$ to form nitric acid (HNO_3), one can calculate NO_x production rates based on the estimated surface flux F_{NO_x} with

$$\frac{d\text{NO}_x}{dt} \sim \frac{F_{\text{NO}_x}}{H} - k_{\text{NO}_2}[\text{NO}_2] + [\text{OH}] \quad (7)$$

We assume boundary layer depths H of 250 m during the day based on previous sodar records (Argentini et al., 2005) and 10 m during night time following the estimate after Pollard et al. (1973). The resulting mixing time scales, H/u_* , of 27 and 6 minutes, respectively, are again relatively short in comparison to reported NO_x lifetimes on the Plateau and justify to a first order the assumption of uniform mixing. The reaction constant $k_{\text{NO}_2+\text{OH}}$ is calculated for Dome C conditions according to recommendations listed in Sander et al. (2006). Measured NO_2 is used, whereas OH is set to a constant value of $2.0 \times 10^6 \text{ molecule cm}^{-3}$, which corresponds to the 16-31 December mean at South Pole in 1998 and 2000 (Eisele et al., 2008). Average NO_x production rates of 4 and 98 pptv hr^{-1} are obtained at local noon (1130-1230 LT) and midnight (2330-0030 LT), respectively. This indicates that the increase in boundary layer depth during the day offsets by far the concurrent increase in snow emission flux. Chemical loss rates from the right hand term in Eq. 7 depended here mostly on NO_2 (Fig. 7b) and were therefore smaller during the day (3 pptv hr^{-1}) than during the night (13 pptv hr^{-1}). The night time NO_x production rate is of the order of magnitude needed to explain the steep evening rise of NO_x concentrations from 110 to 300 pptv in about 2 h (Fig. 9a). These results are sensitive to the choice of mixing depth, but suggest that the photolytic snow source has a significant impact on atmospheric NO_x concentrations, especially during times of the day when the boundary layer is compressed (Fig. 9). This is also consistent with independent measurements of the stable isotopic composition of atmospheric particulate nitrate at Dome C which show on a seasonal time scale a clear signature of snow emissions from nitrate photolysis (Frey et al., 2009b).

A quantitative description of the NO_x snow source is not only important for the understanding of atmospheric boundary layer chemistry above snow surfaces but also for the interpretation of the nitrate record preserved in ice cores. Relevant processes

include snow nitrate photolysis, physical transport and mixing of the main photolysis products and chemical reactions. Comparisons of published flux measurements from different sites and model calculations both can help to derive model parameterizations of NO_x emissions from snow.

5 For example, average and noon time NO_x flux estimated at Halley on 2–Feb 2005 were 7.3×10^{12} and 12.6×10^{12} molecule $\text{m}^{-2}\text{s}^{-1}$, respectively (Bauguitte et al., 2012). However, the latter study simplified flux estimates by linearizing the logarithmic concentration profile, which can induce significant error depending on the inlet heights. Recalculation of the Halley data with Eq. 5 for neutral conditions yields $\sim 20\%$ smaller values,
10 i.e. 5.9×10^{12} and 10.2×10^{12} molecule $\text{m}^{-2}\text{s}^{-1}$, respectively. At South Pole (2835 m) average NO_x flux during 26–30 Nov 2000 was 3.9×10^{12} molecule $\text{m}^{-2}\text{s}^{-1}$ (Oncley et al., 2004). It should be borne in mind that this study measured only NO gradients and inferred NO_x flux based on atmospheric photochemical considerations (Oncley et al., 2004). Thus, it appears that the seasonal and noon time average NO_x flux at Dome C
15 of 6.9×10^{12} and 9.4 molecule $\text{m}^{-2}\text{s}^{-1}$ (Table 3) belong to the largest values reported so far from Antarctica and even the Arctic (see overview in Bauguitte et al., 2012). However, the use of inter-site comparisons to test the current model of the NO_x snow source remains difficult since instrumentation and methods to estimate flux vary considerably in between sites (e.g. Bauguitte et al., 2012).

20 In the following, observed NO_x flux is compared with a simple model that calculates potential NO_2 production rates from the main NO_3^- photolysis channel (R8) for Dome C conditions. Briefly, the radiation transfer model TUV-snow (Lee-Taylor and Madronich, 2002) was constrained with measured snow optical properties and actinic flux to calculate depth-resolved photolysis rates of nitrate in snow, $j_{\text{NO}_3^-}$, for reaction
25 R8 (France et al., 2011). For the latter, published absorption cross sections of aqueous nitrate $\sigma_{\text{NO}_3^-}$ and quantum yield of NO_3^- on ice are used (Chu and Anastasio, 2003). The values of $j_{\text{NO}_3^-}$ and measured profiles of nitrate concentration in the top 1 m of snow allow computation of a depth integrated NO_2 flux, which yielded a median of 3.7×10^{12} molecule $\text{m}^{-2}\text{s}^{-1}$ during 18 Dec 2009–21 Jan 2010 or $\sim 69\%$ of the observed

median flux of NO_x (Table 2).

Comparison of the respective diurnal cycles suggests that the discrepancy between model and observations is due to underprediction of observations during night time, whereas NO_2 flux modelled during early morning to noon time matches measured NO_x emissions quite well (Fig. 9b). This suggests that a rather simplistic model, which assumes NO_2 to be the main NO_3^- photolysis product (Grannas et al., 2007) and neglects any secondary chemistry or transport processes, can predict noon time NO_x emissions from snow at Dome C. The mismatch during the remainder of the day highlights existing uncertainties in the parameterization of the NO_x snow source:

Firstly, the dynamics of vertical chemical exchange do not affect average daily values, but determine the shape of the diurnal NO_x flux cycle. For example, the observed night time increase in wind shear potentially drives ventilation of NO_x which had been temporarily accumulated in the upper snow pack during very stable conditions to the air above it.

Secondly, nitrite (NO_2^-) has been proposed to have the potential to contribute to NO_x emissions from snow (Chu and Anastasio, 2007). Surface snow at Dome C was analysed repeatedly for NO_2^- during the 2010-11 field season. The effect of chemical loss was minimised by placing the sampled snow into bottles already containing the reagents used for analysis, but concentrations were consistently below the LOD of 0.5 ppbw. A major contribution from NO_2^- to the NO_x flux seems therefore less likely, but could still explain part of the flux discrepancy.

Thirdly, the quantum yield of NO_3^- photolysis in natural snow is not well known. It characterises the so-called cage effect, i.e. the tendency of the ice matrix to trap reaction products, and can have a large influence on flux. A recent lab study found that the quantum yield for photolysis of HNO_3 adsorbed to the surface of ice films is close to unity (Zhu et al., 2010), whereas that of NO_3^- measured by Chu and Anastasio (2003) on artificial ice pellets and used in the model calculation is three orders of magnitude smaller. It follows that the efficiency of nitrate photolysis is highly sensitive to the location of nitrate in the snow grain and its potential range could explain the difference

between observed and calculated NO_x flux.

4.3 The NO_2 :NO ratio and potential radical concentrations

Ratios of atmospheric concentrations of NO_2 and NO observed at Dome C are <1 during daytime and >1 during nighttime, similar to observations at Halley (Fig. 10).

5 Interestingly, they show a height dependency, i.e. values increase between 1.0 and 0.01 m, with maxima in firn air (Fig. 10, Table 2). They can be compared to steady-state ratios predicted by the simple Leighton mechanism (R1-3):

$$\frac{[\text{NO}_2]}{[\text{NO}]} = \frac{k_{\text{R3}}[\text{O}_3]}{j_{\text{NO}_2}} \quad (8)$$

Ozone measurements were available from Concordia station and NO_2 photolysis rates j_{NO_2} were calculated with TUV-snow using observed O_3 columns and assuming a standard atmosphere under clear-sky conditions. Scaling of modeled actinic flux to broad band UV measurements allowed to account for cloudy skies (see also France et al., 2011). Observed ratios are found to deviate significantly from Leighton steady-state, and they do so more strongly than at Halley (Fig. 10).

15 The steady-state assumption might not apply since significant snow emissions predominantly in the form of NO_2 can shift the NO_2 :NO ratio, i.e. converting average NO_x emission flux to a volumetric production rate yields values of the same order of magnitude as NO_2 formation via R3, especially when the air is stably stratified. However, a closer examination of the median ratios reveals that they are very similar at the 1.0 m and 4.0 m level throughout the day, whereas at 0.01 m and in firn air they differ, especially during daytime when the emission flux is at its maximum (Fig. 10). The ratios are therefore suggested to be perturbed by photolytic NO_2 release in firn air and at the snow surface, but likely reach a pseudo steady-state after having diffused some distance away from the snow source, i.e. here to the 1.0 m level.

25 Deviations from steady-state are then due to oxidants other than O_3 such as peroxy and halogen radicals and can be accounted for in an extended Leighton ratio as derived

in Ridley et al. (2000). For small carbon number peroxy radicals (RO_2) $k_{\text{R4}} \sim k_{\text{R6}}$ and for $\text{XO}=\text{BrO}, \text{ClO}$ $k_{\text{R4}} \sim 0.5k_{\text{R7}}$. The ratio can then be written as

$$\frac{[\text{NO}_2]}{[\text{NO}]} = \frac{k_{\text{R3}}[\text{O}_3] + k_{\text{R4}}[\text{OX}]}{j_{\text{NO}_2}} \quad (9)$$

where the total radical concentration $[\text{OX}] = [\text{HO}_2] + [\text{RO}_2] + 2[\text{XO}]$ (Ridley et al., 2000). With the extended Leighton ratio we calculate a season mean for $[\text{OX}]$ of $7.4 \times 10^8 \text{ molecule m}^{-3}$ (38 pptv), which are attributed to radicals if only the above reactions are responsible for the observed shift in $\text{NO}_2:\text{NO}$ ratios. These values are about 9 times the $\text{HO}_2 + \text{RO}_2$ concentrations observed at South Pole (Eisele et al., 2008) and 3 times those seen at Summit (Sjostedt et al., 2007).

Including observed levels of halogen radicals BrO and IO into equation 9 explained the shift in $\text{NO}-\text{NO}_2$ partitioning in coastal Antarctica (Bauguitte et al., 2012). However, even if halogen radicals were occasionally present at Dome C, coastal levels of ~ 5 pptv would be too low to explain a significant part of the inferred shift in $\text{NO}_2:\text{NO}$. Thus, the ratios suggest that peroxy radical levels in the boundary layer of Dome C are either significantly higher than measured elsewhere in the polar regions or other processes leading to elevated NO_2 have to be invoked.

5 Conclusions

First-time observations of both nitrogen oxides, NO and NO_2 in ~~the interior of~~ Antarctica confirm previous findings at South Pole that NO_x mixing ratios in the regional lower troposphere are highly elevated compared to coastal Antarctica. The average NO_x levels at Dome C appear to be typical for the summer boundary layer of the larger EAIS region as a comparison with NO measurements from a recent airborne campaign suggests (Slusher et al. (2010), Table 3). Meaningful site inter-comparisons of NO_x and other chemical species need to take into account not only season or latitude but also

measurement height, since vertical gradients of mixing ratios can be significant, especially during times when the air is stably stratified. A steady-state analysis of $\text{NO}_2:\text{NO}$ ratios indicates potentially large mixing ratios of peroxy radicals in the air above the snow ~~confirming~~ the existence of an oxidising canopy enshrouding the East Antarctic Plateau.

The asymmetry in the characteristic diurnal cycle of NO_x mixing ratios at Dome C, i.e. a maximum in the early evening but lack thereof in the morning, is explained as follows: a convective boundary layer develops from the early morning hours reaching maximum heights around mid day. Efficient convective upward mixing of NO_x snow pack emissions and the concurrent increase in boundary layer height prevent build up of vertical gradients and a pronounced maximum in NO_x mixing ratios. Contrary to that, in the early evening strong radiative cooling and temporary decrease in wind shear during the decay of the convective boundary layer lead to significant accumulation of NO_x mixing ratios from snow emissions above the snow surface. This is supported by strong vertical gradients of mixing ratios and a measured NO_x snow emission flux on the order of magnitude needed to explain the rapid increase in mixing ratios when the boundary layer becomes very shallow (Fig. 9). It is possible that a highly non-linear $\text{HO}_x\text{-NO}_x$ system as seen at South Pole forms at Dome C on a daily basis. Later in the evening a small increase of wind shear gives rise to increases in atmospheric diffusivity and NO_x emission flux, again consistent with observed reductions in gradients of NO_x mixing ratios and temperature (Fig. 5, 9). In summary, a strong diurnal cycle of atmospheric mixing ratios of NO_x and likely any other chemical tracer with a surface source is driven by the diffusivity and height of the boundary layer, with the former controlling vertical flux of snow emissions.

The questions arises how representative the diurnal NO_x cycle is for the EAIS Plateau region. The diurnal radiative forcing at Dome C is at the upper end of the range possible on EAIS, while South Pole is a geographical singularity with no diurnal variability at all. It has been argued previously that the convective boundary layer observed at Dome C is not typical for the larger EAIS, as daytime convection will always grow weaker both

North and South of 75° S (King et al., 2006). This ~~implies that also~~ the diurnal variation in boundary layer height is dampened leading to a less extreme diurnal amplitude in NO_x mixing ratios when moving away from Dome C. While the NO_x mixing ratio cycle at DC might be an extreme case, the above confirms the assertion that modelling of atmospheric variability of a chemical species with a significant photochemical or physical surface source requires an accurate description of atmospheric boundary layer dynamics. Accurate model representation of boundary layer physics above the polar ice sheets will not only benefit 1-D atmosphere–snow models to match boundary layer structure, chemical composition and flux above snow (e.g. Thomas et al., 2011; Brun et al., 2011), but also global climate models (e.g. Genthon et al., 2010).

Currently known factors of elevated NO_x above the East Antarctic Plateau region in summer are 24 h of continuous sunlight, a shallow boundary layer, location at the bottom of a large air drainage basin and low temperatures leading to low primary production rates of HO_x radicals (Davis et al., 2008). In addition, NO_x emissions from snow at Dome C are among the highest observed in Antarctica and the Arctic, and thereby contribute also to high levels of NO_x. In particular, the average observed NO_x flux is found to significantly exceed that predicted by a simple nitrate photolysis model. The main uncertainties being able to explain this discrepancy are contributions from nitrite photolysis in snow and the quantum yield of nitrate photolysis in the natural snow pack. They will need to be reduced in the future to update parameterizations of snow denitrification in regional and global chemistry-climate models to represent correctly the NO_x snow source above Antarctica.

For example, calculations with the same nitrate photolysis model suggested that at Dome C up to 80% of nitrate can be removed by photolysis from surface snow (France et al., 2011). We repeated the model calculation but scaled the potential NO₂ emission flux to the observed daily mean NO_x flux. This increased the maximum fraction of nitrate loss due to photolysis to >0.9, closer to observations (Röthlisberger et al., 2002; Frey et al., 2009b). Accurate NO_x flux data are key to explain the observed nitrate loss and concurrent isotope enrichment in Antarctic surface snow (Röthlisberger et al.,

2002; Frey et al., 2009b), which in turn will improve interpretation of the nitrate ice core record.

Future work will include a more detailed comparison between NO_x flux observations and model calculations to improve the parameterization of the snow source of NO_x .

5 Acknowledgements. This work has been made possible thanks to partial support by Institut Paul Émile Victor (IPEV - Programme 1011 NITEDC). MMF is funded by the Natural Environment Research Council through the British Antarctic Survey Polar Science for Planet Earth Programme. We acknowledge also support by the French national atmospheric program LEFE-CHAT managed by INSU/CNRS. Sonic data were provided by C. Genthon, LGGE (IPEV -
10 Programme 1013 and OSUG CENACLAM observatory) and Eric Fossat, OCA. We thank B. Jourdain and the IPEV - Programme CESOA for providing ozone data, PNRA for meteorological data and IPEV for logistic support. JLF & MDK wish to thank NERC for support under grants NE/F0004796/1 and NE/F010788 and NERC FSF through grants S55.0608 & S84.0609 & RHUL research strategy fund awards.

15 References

- Anderson, P. S. and Neff, W. D.: Boundary layer physics over snow and ice, *Atmos. Chem. Phys.*, 8(13), 3563–3582, 2008.
- Argentini, S., Viola, A., Sempreviva, A. M., and Petenko, I.: Summer boundary-layer height at the plateau site of Dome C, Antarctica, *Bound.-Lay. Meteorol.*, 115(3), 409–422, doi:10.1007/s10546-004-5643-6, 2005.
- 20 Bauguitte, S. J.-B., Bloss, W. J., Evans, M. J., Salmon, R. A., Anderson, P. S., Jones, A. E., Lee, J. D., Saiz-Lopez, A., Roscoe, H. K., Wolff, E. W., and Plane, J. M. C.: Summertime NO_x measurements during the CHABLIS campaign: can source and sink estimates unravel observed diurnal cycles?, *Atmos. Chem. Phys.*, 12(2), 989–1002, doi:10.5194/acp-12-989-2012, 2012.
- 25 Brun, E., Six, D., Picard, G., Vionnet, V., Arnaud, L., Bazile, E., Boone, A., Bouchard, A., Genthon, C., Guidard, V., Le Moigne, P., Rabier, F., and Seity, Y.: Snow/atmosphere coupled simulation at Dome C, Antarctica, *J. Glaciol.*, 57(204), 721–736, doi:10.3189/002214311797409794, 2011.

- Chu, L. and Anastasio, C.: Quantum yields of hydroxyl radical and nitrogen dioxide from the photolysis of nitrate on ice, *J. Phys. Chem. A*, 107(45), 9594–9602, 2003.
- Chu, L. and Anastasio, C.: Temperature and wavelength dependence of nitrite photolysis in frozen and aqueous solutions, *Environ. Sci. Technol.*, 41, 3626–3632, doi:10.1021/es062731q, 2007.
- Cohen, L., Helmig, D., Neff, W. D., Grachev, A. A., and Fairall, C. W.: Boundary-layer dynamics and its influence on atmospheric chemistry at Summit, Greenland, *Atmos. Environ.*, 41(24), 5044–5060, doi:10.1016/j.atmosenv.2006.06.068, 2007.
- Crawford, J. H., Davis, D. D., Chen, G., Buhr, M., Oltmans, S., Weller, R., Mauldin, L., Eisele, F., Shetter, R., Lefer, B., Arimoto, R., and Hogan, A.: Evidence for photochemical production of ozone at the South Pole surface, *Geophys. Res. Lett.*, 28(19), 3641–3644, 2001.
- Davis, D. D., Chen, G., Buhr, M., Crawford, J., Lenschow, D., Lefer, B., Shetter, R., Eisele, F., Mauldin, L., and Hogan, A.: South Pole NO_x chemistry : an assessment of factors controlling variability and absolute levels, *Atmos. Environ.*, 38(32), 5275–5388, doi:10.1016/j.atmosenv.2004.04.039, 2004a.
- Davis, D. D., Eisele, F., Chen, G., Crawford, J., Huey, G., Tanner, D., Slusher, D., Mauldin, L., Oncley, S., Lenschow, D., Semmer, S., Shetter, R., Lefer, B., Arimoto, R., Hogan, A., Grube, P., Lazzara, M., Bandy, A., Thornton, D., Berresheim, H., Bingemer, H., Hutterli, M., McConnell, J., Bales, R., Dibb, J., Buhr, M., Park, J., McMurry, P., Swanson, A., Meinardi, S., and Blake, D.: An overview of ISCAT 2000, *Atmos. Environ.*, 38, 5363–5373, doi:10.1016/j.atmosenv.2004.05.037, 2004b.
- Davis, D. D., Seelig, J., Huey, G., Crawford, J., Chen, G., Wang, Y. H., Buhr, M., Helmig, D., Neff, W., Blake, D., Arimoto, R., and Eisele, F.: A reassessment of Antarctic plateau reactive nitrogen based on ANTCI 2003 airborne and ground based measurements, *Atmos. Environ.*, 42, 2831–2848, doi:10.1016/j.atmosenv.2007.07.039, 2008.
- Eisele, F., Davis, D. D., Helmig, D., Oltmans, S. J., Neff, W., Huey, G., Tanner, D., Chen, G., Crawford, J., Arimoto, R., Buhr, M., Mauldin, L., Hutterli, M., Dibb, J., Blake, D., Brooks, S., Johnson, B., Roberts, J. M., Wang, Y., Tan, D., and Flocke, F.: Antarctic Tropospheric Chemistry Investigation (ANTCI) 2003 overview, *Atmos. Environ.*, 42(12), 2749–2761, 2008.
- France, J. L., King, M. D., Frey, M. M., Erbland, J., Picard, G., Preunkert, S., MacArthur, A., and Savarino, J.: Snow optical properties at Dome C (Concordia), Antarctica; implications for snow emissions and snow chemistry of reactive nitrogen, *Atmos. Chem. Phys.*, 11(18), 9787–9801, doi:10.5194/acp-11-9787-2011, 2011.

- Frey, M. M., Stewart, R. W., McConnell, J. R., and Bales, R. C.: Atmospheric hydroperoxides in West Antarctica: links to stratospheric ozone and atmospheric oxidation capacity, *J. Geophys. Res.*, 110, D23301, doi:10.1029/2005JD006110, 2005.
- 5 Frey, M. M., Hutterli, M. A., Chen, G., Sjostedt, S. J., Burkhardt, J. F., Friel, D. K., and Bales, R. C.: Contrasting atmospheric boundary layer chemistry of methylhydroperoxide (CH_3OOH) and hydrogen peroxide (H_2O_2) above polar snow, *Atmos. Chem. Phys.*, 9(10), 3261–3276, 2009a.
- Frey, M. M., Savarino, J., Morin, S., Erbland, J., and Martins, J. M. F.: Photolysis imprint in the nitrate stable isotope signal in snow and atmosphere of East Antarctica and implications for reactive nitrogen cycling, *Atmos. Chem. Phys.*, 9, 8681–8696, 2009b.
- 10 Genthon, C., Town, M. S., Six, D., Favier, V., Argentini, S., and Pellegrini, A.: Meteorological atmospheric boundary layer measurements and ECMWF analyses during summer at Dome C, Antarctica, *J. Geophys. Res.*, 115, D05104, doi:10.1029/2009JD012741, 2010.
- Grannas, A. M., Jones, A. E., Dibb, J., Ammann, M., Anastasio, C., Beine, H. J., Bergin, M. H., Bottenheim, J., Boxe, C., Carver, G., Chen, G., Domine, F., Frey, M., Guzman, M. I., Heard, D. E., Helmig, D., Hoffmann, M. R., Honrath, R., Huey, G., Hutterli, L. M., Jacobi, H. W., Klan, P., McConnell, J., Sander, R., Savarino, J., Shepson, P., Simpson, W., Sodeau, J., von Glasow, R., Weller, G., Wolff, E., and Zhu, T.: An overview of snow photochemistry: evidence, mechanisms and impacts, *Atmos. Chem. Phys.*, 7, 4329–4373, 2007.
- 20 Helmig, D., Boulter, J., David, D., Birks, J. W., Cullen, N. J., Steffen, K., Johnson, B. J., and Oltmans, S. J.: Ozone and meteorological boundary-layer conditions at Summit, Greenland, during 3–21 June 2000, *Atmos. Environ.*, 36(15–16), 2595–2608, 2002.
- Hoegstroem, U.: Non-dimensional wind and temperature profiles in the atmospheric surface layer: a re-evaluation, *Bound.-Lay. Meteorol.*, 42, 55, 1988.
- 25 Honrath, R. E., Peterson, M. C., Dziobak, M. P., Dibb, J., Arsenault, M. A., and Green, S. A.: Release of NO_x from sunlight-irradiated midlatitude snow, *Geophys. Res. Lett.*, 27, 2237–2240, 2000.
- Jacobson, M. Z.: *Fundamentals of Atmospheric Modeling*, Cambridge University Press, 1999.
- Jones, A. E., Wolff, E. W., Salmon, R. A., Bauguutte, S. J.-B., Roscoe, H. K., Anderson, P. S., Ames, D., Clemitshaw, K. C., Fleming, Z. L., Bloss, W. J., Heard, D. E., Lee, J. D., Read, K. A., Hamer, P., Shallcross, D. E., Jackson, A. V., Walker, S. L., Lewis, A. C., Mills, G. P., Plane, J. M. C., Saiz-Lopez, A., Sturges, W. T., and Worton, D. R.: Chemistry of the Antarctic Boundary Layer and the Interface with Snow: an overview of the CHABLIS

- campaign, *Atmos. Chem. Phys.*, 8(14), 3789–3803, 2008.
- Jones, A. E., Wolff, E. W., Ames, D., Bauguitte, S. J.-B., Clemitshaw, K. C., Fleming, Z., Mills, G. P., Saiz-Lopez, A., Salmon, R. A., Sturges, W. T., and Worton, D. R.: The multi-seasonal NO_y budget in coastal Antarctica and its link with surface snow and ice core nitrate: results from the CHABLIS campaign, *Atmos. Chem. Phys.*, 11(17), 9271–9285, doi:10.5194/acp-11-9271-2011, 2011.
- Kaimal, J. and Finnigan, J. J.: *Atmospheric Boundary Layer Flows*, Oxford University Press, 1994.
- Kerbrat, M., Legrand, M., Preunkert, S., Gallée, H., and Kleffmann, J.: Nitrous acid at Concordia (inland site) and Dumont d’Urville (coastal site), East Antarctica, *J. Geophys. Res.*, 117, D08 303, doi:10.1029/2011JD017149, 2012.
- King, J. C. and Anderson, P. S.: Heat and water vapor fluxes and scalar roughness lengths over an Antarctic ice shelf, *Bound.-Lay. Meteorol.*, 69, 101–121, 1994.
- King, J. C., Argentini, S. A., and Anderson, P. S.: Contrasts between the summertime surface energy balance and boundary layer structure at Dome C and Halley stations, Antarctica, *J. Geophys. Res.*, 111, D02 105, doi:10.1.1029/2005JD006130, 2006.
- Kuhn, H., Lettau, H., and Riordan, A.: Stability-related wind spiraling in the lowest 32 meters, in: *Meteorological Studies at Plateau Station, Antarctica*, edited by Businger, J., vol. 25 of *Antarct. Res. Ser.*, pp. 93–111, AGU, Washington D.C., 1977.
- Lee-Taylor, J. and Madronich, S.: Calculation of actinic fluxes with a coupled atmosphere-snow radiative transfer model, *J. Geophys. Res.*, 107, D24, 4796, doi:10.1029/2002JD002084, 2002.
- Legrand, M., Preunkert, S., Jourdain, B., Gallée, H., Goutail, F., Weller, R., and Savarino, J.: Year-round record of surface ozone at coastal (Dumont d’Urville) and inland (Concordia) sites in East Antarctica, *J. Geophys. Res.*, 114, D20 306, doi:10.1029/2008JD011667, 2009.
- Leighton, P. A.: *Photochemistry of air pollution*, Academic Press, New York, 1961.
- Lenschow, D. H.: Micrometeorological techniques for measuring biosphere-atmosphere trace gas exchange, in: *Biogenic Trace Gases: Measuring emissions from soil and water*, edited by Matson, P. A. and Harriss, R. C., pp. 126–163, Blackwell Science, London, 1995.
- Liao, W., Case, A. T., Mastromarino, J., Tan, D., and Dibb, J. E.: Observations of HONO by laser-induced fluorescence at the South Pole during ANTCI 2003, *Geophys. Res. Lett.*, 33(9), L09 810, doi:10.1029/200GL025470, 2006.
- Neff, W., Helmig, D., Grachev, A., and Davis, D.: A study of boundary layer behavior associated with high NO concentrations at the South Pole using a minisodar, tethered balloons and sonic

- anemometer, *Atmos. Environ.*, 42(12), 2762–2779, doi:10.1016/j.atmosenv.2007.01.033, 2008.
- Onclay, S. P., Buhr, M., Lenschow, D. H., Davis, D., and Semmer, S. R.: Observations of summertime NO fluxes and boundary-layer height at the South Pole during ISCAT 2000 using scalar similarity, *Atmos. Environ.*, 38(32), 5389–5398, doi:10.1016/j.atmosenv.2004.05.053, 2004.
- Pollard, R., Rhines, P. B., and Thompson, R.: The deepening of the wind-mixed layer, *Geophys. Fluid Dyn.*, 3, 381–404, 1973.
- Ridley, B. A., Walega, J., Montzka, D., and et al.: Is the Arctic surface layer a source and sink of NO_x in winter/spring, *J. Atmos. Chem.*, 36, 1–22, 2000.
- Röthlisberger, R., Hutterli, M. A., Wolff, E. W., Mulvaney, R., Fischer, H., Bigler, M., Goto-Azuma, K., Hansson, M. E., Ruth, U., Siggaard-Andersen, M. L., and Steffensen, J. P.: Nitrate in Greenland and Antarctic ice cores: a detailed description of post-depositional processes, *Ann. Glaciol.*, 35, 209–216, 2002.
- Ryerson, T. B., Williams, E. J., and Fehsenfeld, F. C.: An efficient photolysis system for fast-response NO₂ measurements, *J. Geophys. Res.*, 105(D21), 26 447–26 461, 2000.
- Sander, S. P., Friedl, R. R., Golden, D. M., Kurylo, M. J., Moortgat, G. K., Wine, P. H., Ravishankara, A., Kolb, C. E., Molina, M., Finlayson-Pitts, B. J., Huie, R. E., and Orkin, V. L.: Chemical Kinetics and Photochemical Data for Use in Atmospheric Studies, Tech. Rep. Eval. No. 15, Jet Propulsion Laboratory, 2006.
- Sjostedt, S. J., Huey, L. G., Tanner, D. J., Peischl, J., Chen, G., Dibb, J. E., Lefer, B., Hutterli, M. A., Beyersdorf, A. J., Blake, N. J., Blake, D. R., Sueper, D., Ryerson, T., Burkhardt, J., and Stohl, A.: Observations of hydroxyl and the sum of peroxy radicals at Summit, Greenland during summer 2003, *Atmos. Environ.*, 41, 5122–5137, 2007.
- Slusher, D. L., Neff, W. D., Kim, S., Huey, L. G., Wang, Y., Zeng, T., Tanner, D. J., Blake, D. R., Beyersdorf, A., Lefer, B. L., Crawford, J. H., Eisele, F. L., Mauldin, R. L., Kosciuch, E., Buhr, M. P., Wallace, H. W., and Davis, D. D.: Atmospheric chemistry results from the ANTCI 2005 Antarctic plateau airborne study, *J. Geophys. Res.*, 115(D07304), doi:10.1029/2009JD012605, 2010.
- Thomas, J. L., Stutz, J., Lefer, B., Huey, L. G., Toyota, K., Dibb, J. E., and von Glasow, R.: Modeling chemistry in and above snow at Summit, Greenland – Part 1: Model description and results, *Atmos. Chem. Phys.*, 11(10), 4899–4914, doi:10.5194/acp-11-4899-2011, 2011.
- Van Dijk, A., Moen, A., and De Bruin, H.: The principles of surface flux physics: theory, practice and description of the ECPACK library, Internal Report 2004/1, Meteorology and

Air Quality Group, Wageningen University, Wageningen, The Netherlands, 2006.

- Zhu, C. Z., Xiang, B., Chu, L. T., and Zhu, L.: 308 nm Photolysis of Nitric Acid in the Gas Phase, on Aluminum Surfaces, and on Ice Films, *J. Phys. Chem. A*, 114(7), 2561–2568, doi:10.1021/jp909867a, 2010.
- 5 Zilitinkevitch, S., Baklanov, A., Rost, J., Smedman, A., Lykosov, V., and Calanca, P.: Calculation of the height of the stable boundary layer in practical applications, *Bound.-Lay. Meteorol.*, 105, 389–409, 2002.

Table 1. Overview of parameters characterizing CLD instrument performance at Dome C.

Parameter ^a	NO	NO ₂	N ^b
NO sensitivity, Hz pptv ⁻¹	4.5 (4.4–4.7)	2.5 (2.1–3.0)	23 (CLD1) / 35 (CLD2)
artefact ^c	37 Hz (7–10 pptv)	8 Hz (3–4) pptv	29
CE ^d	–	0.30 (0.25–0.35)	64
random error, pptv	2 (1-12)	11 (5-67)	all data
precision, %	2.5	43.6	all data
HONO interference ^e	–	0.22	–

^amean (range)

^b number of data points included

^cduring 11-Dec 2009 – 3-Jan 2010, after that about half that value, but not used for correction (see text). The range is based on the observed variability in sensitivity

^dphotolytic conversion efficiency of NO₂

^emaximum theoretical interference of HONO in the NO₂ signal (see text)

Table 2. NO_x mixing ratios and flux at Dome C between 22-Dec-2009 and 28-Jan-2010.

Parameter	z, m	mean±1σ	median	maximum	t _{total} , days ^a
NO, pptv	1.0 ^b	111±89	84	565	23.2
	firn	222±214	143	3043	4.4
	0.01	117±93	90	774	12.6
	1.0	102±79	82	565	13.6
	4.0	85±48	77	298	7.7
NO ₂ , pptv	1.0 ^b	102±88	74	616	21.1
	firn	336±284	229	3051	4.4
	0.01	98±76	74	836	12.2
	1.0	79±69	57	616	12.5
	4.0	65±54	50	463	7.0
NO _x , pptv	1.0 ^b	212±154	161	942	21.0
	firn	559±472	371	5247	4.4
	0.01	213±154	168	1238	12.1
	1.0	183±134	145	860	12.5
	4.0	152±90	135	630	7.0
NO ₂ :NO	1.0 ^b	1.2±1.7	0.8	87	21.0
	firn	1.8±1.1	1.5	18.5	4.4
	0.01	1.0±0.9	0.8	17.4	12.1
	1.0	0.9±1.2	0.7	83	12.5
	4.0	0.9±1.1	0.7	40	7.0
F-NO _x × 10 ¹² molecule m ⁻² s ⁻¹	0.01-1.0	6.9±7.2	5.4	73.6	9.4
”, local noon	0.01-1.0	9.4±8.7	9.4	32.2	–
”, local midnight	0.01-1.0	6.2±7.3	2.8	37.9	–
F-NO ₂ × 10 ¹² molecule m ⁻² s ^{-1c}	–	4.3±2.9	3.7	10.6	–
”, local noon	–	8.9±0.4	9.0	10.4	–
”, local midnight	–	0.8±0.2	0.8	1.2	–

^aTotal sample time estimated as the sum of all 1-min intervals

^b10 Dec 2009 to 28 Jan 2010

^cmodelled potential NO₂ production during 18-Dec-2009 to 21-Jan-2010 (see text)

Table 3. Median NO mixing ratios (pptv) on the Antarctic Plateau.

Site	z, m	Nov 16–30	Dec 1–15	Dec 16–31	Jan 1–15	Jan 16–31
Dome C						
NITEDC 2009 ^a	0.01	–	–	123	86	84
	1.0	–	120	81	78	75
	4.0	–	–	100	77	63
South Pole						
ISCAT 1998 ^b	10.0	–	209	237	–	–
ISCAT 2000 ^b	10.0	93	82	88	–	–
ANTCI 2003 ^b		529	164	76	–	–
ANTCI 2005 ^c	0–50	–	95	–	–	–
	51–150	–	90	–	–	–
	151–500	–	30	–	–	–

^athis study

^bValues from Table 3 in Eisele et al. (2008)

^cValues from Plateau flights of the airborne campaign (Table 3 in Slusher et al. (2010))

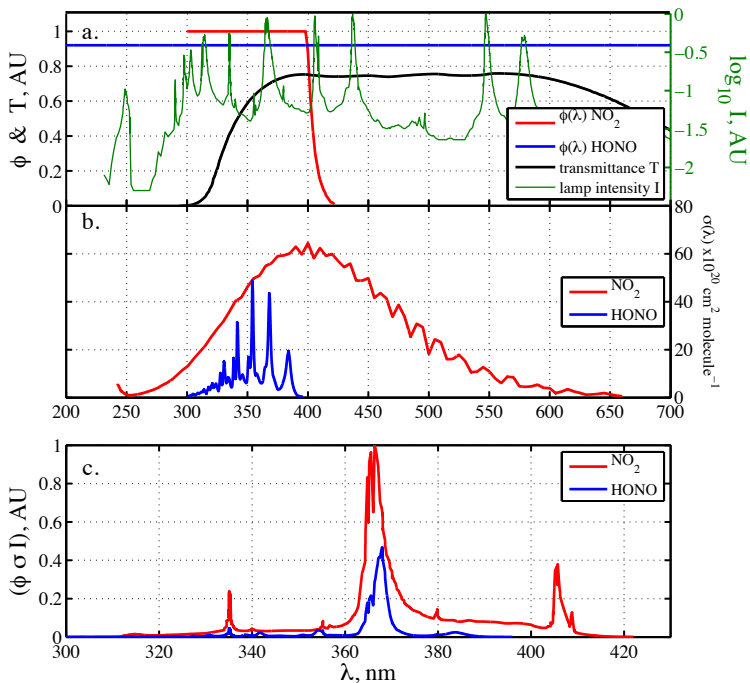


Fig. 1. The potential interference of HONO in the detection of NO_2 was estimated using (a) the relative intensity, I , of the photolytic converter (a 200-W high pressure arc mercury lamp, USHIO-200DP), the respective quantum yields, $\phi(\lambda)$, total transmittance, T , of the optical filters, including a Pyrex window (Oriel, Part No. 60127) and a KBr filter (KG3, Oriel Part No. 51960), (b) the respective absorption cross sections, $\sigma(\lambda)$ (Sander et al., 2006) and (c) $\phi\sigma I$ in order to calculate scaled photolysis rates $j = \int \phi\sigma I d\lambda$. Note different scale of x-axis in (c) and **AU** for arbitrary units.

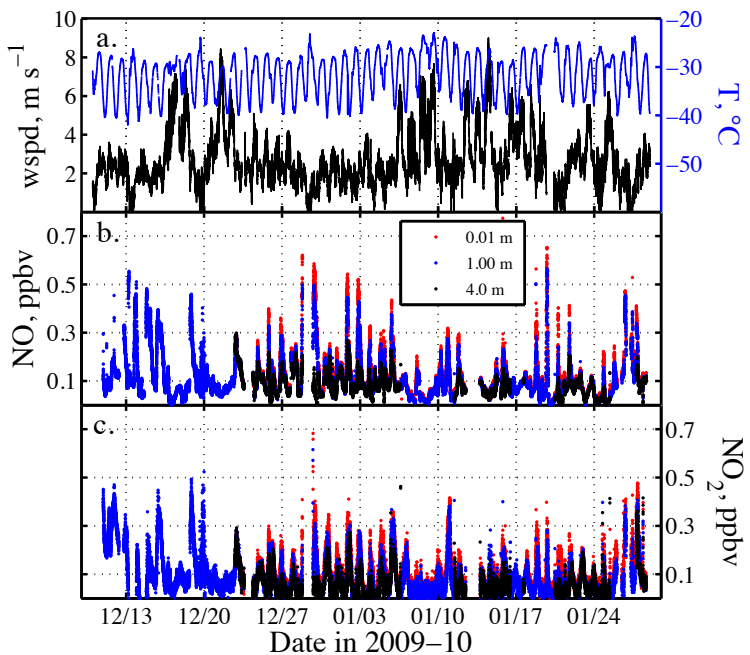


Fig. 2. Overview of atmospheric nitrogen oxide mixing ratios at three heights above the snow and meteorological conditions at Dome C in summer 2009-10.

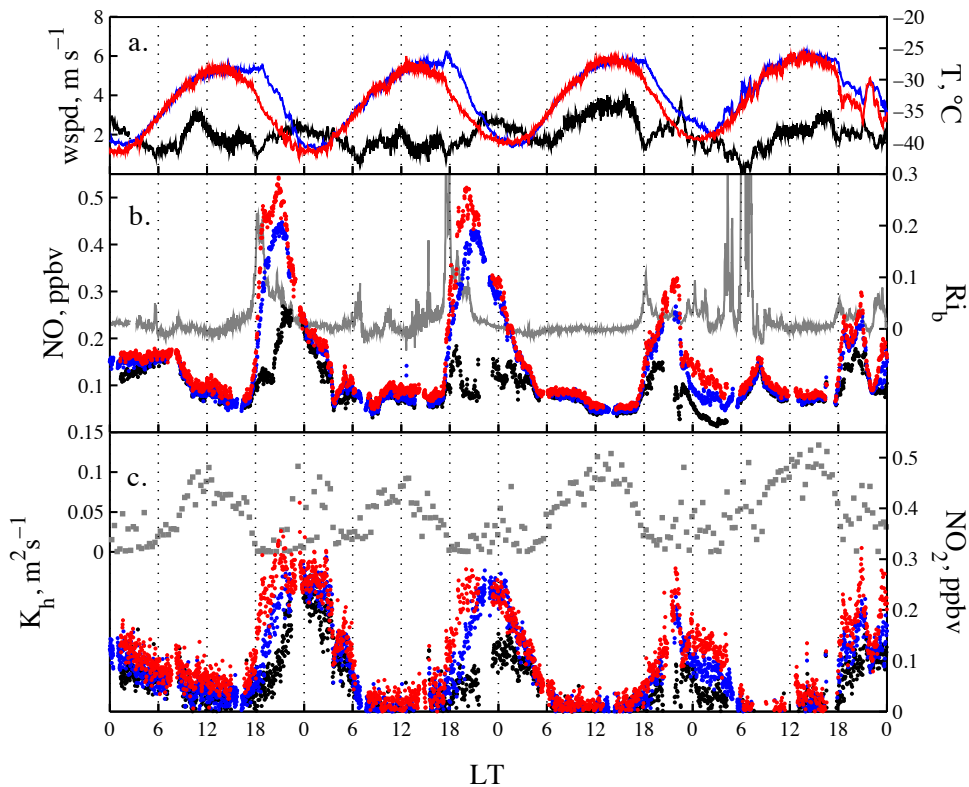


Fig. 3. Diurnal variability from 1 to 4 January 2010: (a) wind speed at 3 m (black line), air temperature at 1 m (blue line) and surface temperature of snow (red line), (b) NO mixing ratios at three heights and bulk Richardson number (grey line) and (c) NO₂ mixing ratios at three heights and turbulent diffusion coefficient of heat at 1 m (grey symbols). Mixing ratios from 0.01, 1.0 and 4.0 m are shown as red, blue and black symbols, respectively.

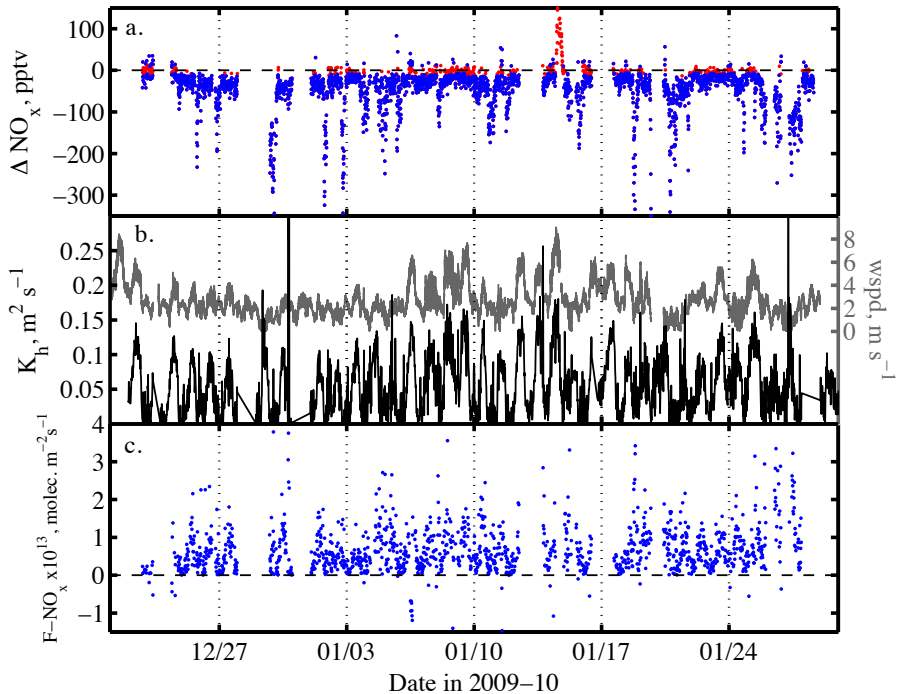


Fig. 4. Estimates of NO_x surface flux at Dome C in summer 2009-10 based on 10-min averages: (a) difference in mixing ratios between 1.0 and 0.01 m (blue symbols); values within ± 1 -std error were excluded from the flux calculation (red symbols), (b) turbulent diffusion coefficient of heat at 1 m and wind speed, and (c) the **molecular** flux of NO_x .

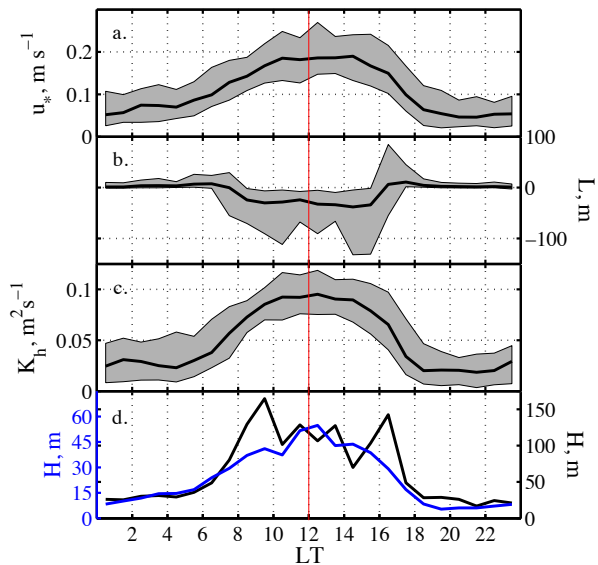


Fig. 5. The asymmetry in the diurnal variability of atmospheric boundary layer parameters with respect to local noon (red line): a) friction velocity u_* , b) Monin-Obukhov length L , c) turbulent diffusion coefficient of heat K_h at 1 m and d) boundary layer height H estimated after Pollard et al. (1973) (blue line) and Zilitinkevitch et al. (2002) (black line); note different y-axis scales. Lines represent median values and shaded areas the range between the 0.25 and 0.75 percentiles of 1-hourly bins from 22-Dec-2009 to 28-Jan-2010.

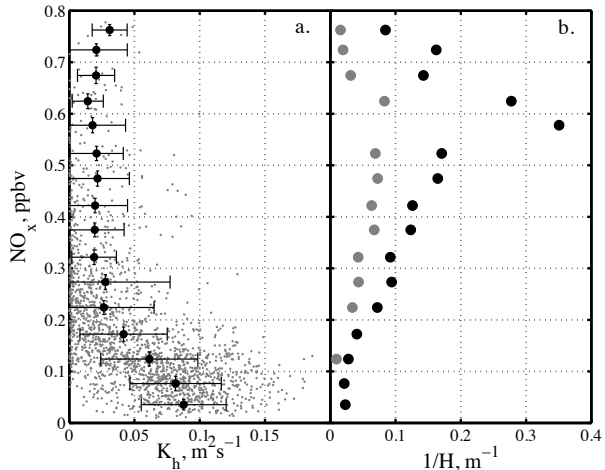


Fig. 6. (a) Atmospheric mixing ratios of NO_x as a function of the turbulent diffusion coefficient of heat K_h (both at 1 m). Plotted are 10-minute means (grey symbols) and data binned into 50 ppbv intervals (means $\pm 1\sigma$ as black symbols and error bars). (b) Binned NO_x mixing ratios as a function of boundary layer height H estimated from equilibrium solutions after Pollard et al. (1973) (black symbols) and Zilitinkevitch et al. (2002) (grey symbols).

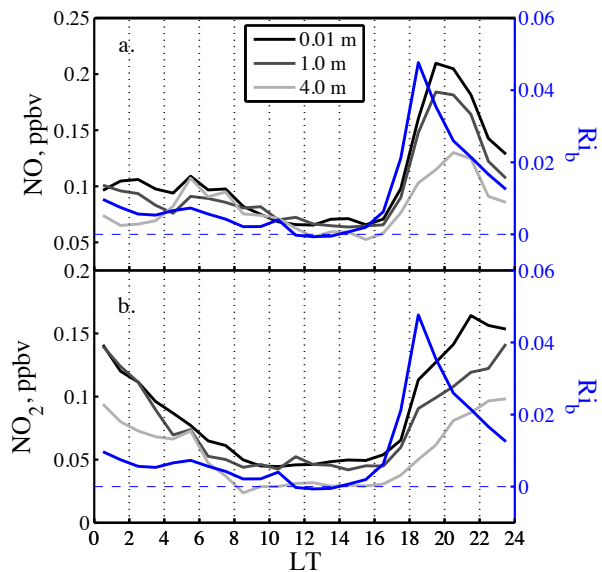


Fig. 7. During 22-Dec-2009 to 28-Jan-2010 the median diurnal cycle of nitrogen oxide mixing ratios at Dome C shows a close association with the bulk Richardson number Ri_b .

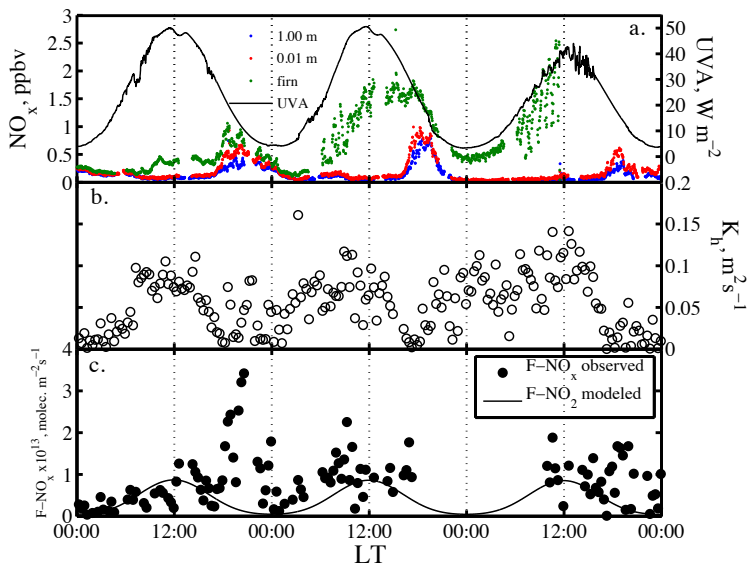


Fig. 8. Atmospheric mixing ratios of NO_x and snow emissions during 18–21 January 2010. Shown are (a) mixing ratios above the snow and in firn air along with UVA irradiance, (b) the turbulent diffusion coefficient of heat K_h at 1 m and (c) observed NO_x flux compared to potential NO_2 flux from nitrate photolysis modelled for Dome C conditions as reported in France et al. (2011).

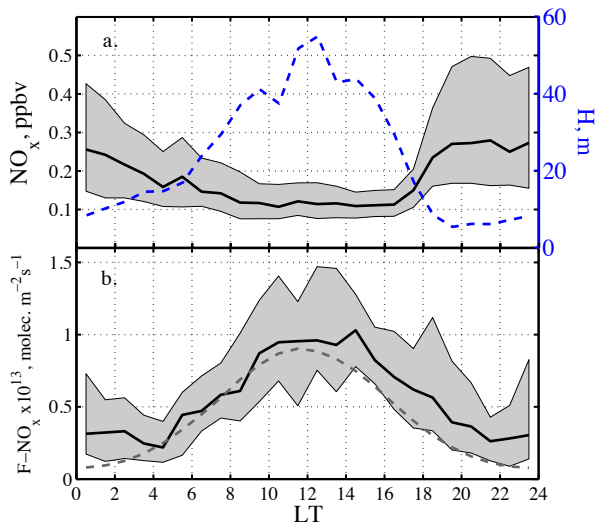


Fig. 9. The median diurnal cycle from 22-Dec-2009 to 28-Jan-2010: (a) NO_x mixing ratios at 1 m with boundary layer height H estimated after Pollard et al. (1973) (blue dashed line) and (b) NO_x flux. Lines represent median values and shaded areas the range between the 0.25 and 0.75 percentiles of 1-hourly bins. The potential NO₂ flux from nitrate photolysis modelled for Dome C conditions by France et al. (2011) is shown for comparison (grey dashed line).

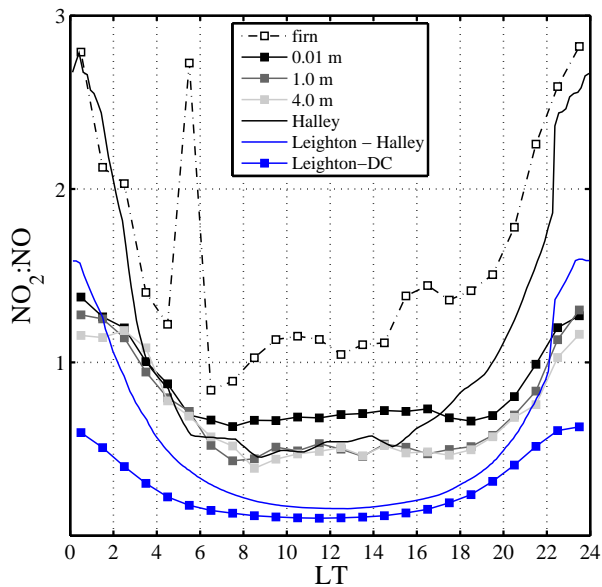


Fig. 10. The median diurnal cycle of the $\text{NO}_2:\text{NO}$ ratio during 22 Dec 2009 to 28 Jan 2010 shows significant deviations from Leighton steady-state at Dome C. Halley observations (black line) are shown for comparison (Bauguitte et al., 2012).